Solar-Terrestrial Physics. 2025. Vol. 11. Iss.1. P. 90–100. DOI: 10.12737/stp-111202511. © 2025
V.L. Yanchukovsky, R.Z. Khisamov. Published by INFRA-M Academic Publishing House

DOI: 10.12737/stp-111202511

Received October 23, 2024
Accepted December 02, 2024

TEMPERATURE EFFECT OF MUONS DETECTED UNDERGROUND BY SCINTILLATION DETECTORS

V.L. Yanchukovsky
A.A. Trofimuk Institute of Oil and Gas Geology and Geophysics SB RAS,
Novosibirsk, Russia, YanchukovskiyVL@ipgg.sbras.ru

R.Z. Khisamov
A.A. Trofimuk Institute of Oil and Gas Geology and Geophysics SB RAS,
Novosibirsk, Russia, KhisamovRZ@ipgg.sbras.ru

Abstract. The A.I. Kuzmin Cosmic Ray Spectrograph in Yakutsk contains a 24-NM-64 neutron monitor and a system of underground MT and SMT muon detectors for recording muons at levels of 0, 7, 20, and 40 m of water equivalent. The temperature effect of muons observed with MT telescopes on gas-discharge counters has been analyzed in the previous work [Yanchukovsky, 2023]. Here we calculate the temperature effect of muons recorded by SMT telescopes. Distributions of the density of temperature coefficients for muons recorded on the surface and at different depths underground were found from SMT telescope data for the period from January 2016 to December 2018, using data on the altitude profile of the atmosphere temperature over Yakutsk for the same period. In the analysis of multidimensional data, we applied the methods of regression on principal components. When constructing a system of linear equations in the space of principal components, we employed the method of projections to latent structures (PLS2). The obtained results were compared with the results of theoretical calculations. The found distributions of the density of temperature coefficients allow us to correctly take into account the temperature effect in data from SMT muon telescopes.

Keywords: cosmic rays, atmosphere, muons, telescope, temperature effect.

INTRODUCTION

The A.I. Kuzmin Cosmic Ray Spectrograph in Yakutsk includes a 24-NM-64 neutron monitor and two complexes of underground muon telescopes (with gas-discharge counters SGM-14 (MT) and scintillation counters ST-301 (SMT) [Gerasimova et al., 2021]), which are installed at levels of 0, 7, 20, and 40 m of water equivalent (m.w.e.) [Starodubtsev et al., 2016]. The receiving characteristics (receiving vectors) have been calculated for the entire complex of instruments [Gerasimova et al., 2021]. Nonetheless, muon intensity variations observed deep in the atmosphere are not only due to variations in the primary cosmic-ray flux outside the atmosphere, but also due to changes in the parameters of the atmosphere itself, which cause barometric and temperature effects of muon intensity. Unlike the barometric effect that is determined by one parameter — the pressure at an observation level, the temperature effect for muons depends on many parameters characterizing atmospheric conditions from the generation layer to the level of muon detection (temperature and mass distribution). To account for the barometric and temperature effects in continuous muon observations with the underground telescope complexes, we have to estimate the magnitude of the effect of these parameters on the muon intensity in the atmosphere. This work has been carried out earlier for muon telescopes with gas-discharge counters SGM-14 [Yanchukovsky, 2023]. Telescopes with scintillation counters ST-301 differ from telescopes with gas-discharge counters SGM-14 both in effective energies of detected muons, as well as in the beam patterns of muon telescopes from zenith and azimuth angles, and a set of zenith and azimuth muon detection directions [Grigoryev el al., 2011; Starodubtsev et al., 2013]. Therefore, significant differences in the density distributions of the temperature coefficients for MT and SMT are not improbable either. Kuzmenko and Yanchukovsky [2015] have shown that the use of multivariate regression (MVR) methods for estimating the density distribution of temperature coefficients is incorrect since temperature variations in different atmospheric layers are correlated. In studying the temperature effect of muons, as previously in [Yanchukovsky, 2023], Principal Component Regression (PCR) methods were applied [Jolliffe, 2002; Principal Manifolds..., 2007]. When constructing a system of linear equations in the space of principal components (PCs), the projection method on latent structures (PLS2) was employed [Esbensen, 2005; Pomerantsev, 2014].

DATA AND THEIR PREPARATION FOR ANALYSIS

The work is based on raw (uncorrected for atmospheric effects and primary variation) hourly data from continuous observations made by muon detectors with scintillation counters ST-301, a neutron monitor, and atmospheric pressure data from January 2016 to December 2018 [https://ikfia.ysn.ru/dannye-lklve, https://ikfia.ysn.ru/data/hecrlab/mt, https://ikfia.ysn.ru/data/hecrlab/ipm]. Altitude profiles of atmospheric temperature (for each hour) over Yakutsk were taken from the database [http://crsa.izmiran.ru/phpmyadmin], which contains the results of the US National Center for Environmental Prediction [https://www.nco.ncep.noaa.gov/pmb/products/gfs]. The given time interval involves the launch and installation of the complex of scintillation telescopes for continuous monitoring; therefore, we thoroughly verified the raw data. We visually monitored the raw data and stability of detection efficiency in the channel, using plots for all recording channels and plots of ratios between identical channels (50N/50S, 50E/50W, 59NE/59SW, 59NW/59SE, 67N/67S, 74N/74S, the number indicates the zenith angle; the letters, the azimuth direction). The detected gaps in the raw hourly data were filled in with the averages calculated from four values both before and after each gap, and outliers in the data were eliminated. When a failure in the efficiency of one of the four identical channels was detected, we corrected the data from this channel for the other three channels. The normalization factor was found using the method of ratios [Shapley, 1969; Yanchukovsky, Filimonov, 1994]. On average, the following number of daily averages has been corrected for all channels of the SMT complex: 0 m.w.e. — 6.8 %, 7 m.w.e. — 7.5 %, 20 m.w.e. — 13.2 %, 40 m.w.e. — 17 %. The raw data is briefly described in Table 1.

The raw data was reduced to daily averages except the data for the 7 m.w.e. level, where observations were initiated somewhat later than at other levels. For the 7 m.w.e. level, we had to use values averaged over half a day since the minimum sample size [Yanchukovsky and Kuzmenko, 2018] should be about 1000 values.

The total number of values was:

- for the telescope on the surface (SMT00) — 956 daily averages;
- for the telescope at the 7 m.w.e. level (SMT07) — 1182 half-day averages;
- for the telescope at the 20 m.w.e. level (SMT20) — 1077 daily averages;
- for the telescope at 40 m.w.e. (SMT40) — 1077 daily averages.

Table 2 lists averages of meteorological parameters and neutron monitor counting rate for each sample.

Then, we centered and normalized the raw data. We determined averages for the entire time interval of interest for each channel of the complex from which the intensity variations (in %) were found. The variables (pressure, surface and mass average temperatures, and temperatures in 16 isobars) were presented as deviations from averages for the same time interval. Figure 1 presents raw observational data for four levels of muon detection.

The raw data (see Figure 1) on observed muon intensity variations contains the barometric effect, the temperature effect of the surface layer (variable mass layer), the integral temperature effect of the entire atmosphere, and variations in primary cosmic rays. From this set it is necessary to single out the temperature component of intensity variations, which is defined by the integral temperature effect of the atmosphere. The statistical model of atmospheric cosmic-ray variations is presented in [Yanchukovsky, Kuzmenko, 2018] as a four-parameter linear multivariate regression equation

$$\delta J_\mu(t) = \beta\Delta h(t) + \alpha_{\text{surf}}\Delta T_{\text{surf}}(t)\times \times\left[h(t)-950\right] + \alpha_{\text{ma}}\Delta T_{\text{ma}}(t) + \gamma\delta J_{\text{n}}(t), \quad (1)$$

where $\delta J_\mu(t) = \dfrac{J_\mu(t)-\bar{J}_\mu}{J_\mu}\cdot 100\ \%$ is the observed muon intensity variation (resulting factor y); $\Delta h = h(t) - h_0$ — atmospheric pressure changes (factor x_1); $\Delta T_{\text{surf}}(t) = T_{\text{surf}}(t) - \bar{T}_{\text{surf}}$ — variable mass surface temperature variations (factor x_2); $\Delta T_{\text{ma}}(t) = T_{\text{ma}}(t) - \bar{T}_{\text{ma}}$ — mass average atmospheric temperature variations (factor x_3); $\delta J_{\text{n}}(t) = \dfrac{J_{\text{n}}(t)-\bar{J}_{\text{n}}}{J_{\text{n}}}\cdot 100\ \%$ — neutron component intensity variations (data from the Yakutsk neutron monitor) corrected for atmospheric pressure changes (factor x_4).

Table 1

Characteristics of raw data

SMT channel	Average counting rates for a level (m.w.e.), hr^{-1}				K	Statistical error in daily averages, %			
	00	07	20	40		00	07	20	40
0Z	1417797	666178	316065	124005	1	0.017	0.025	0.036	0.058
50N	257946	129537	64088	28300	1	0.040	0.057	0.081	0.121
50S	253278	124640	66576	25698	1	0.041	0.058	0.079	0.127
50E	173760	81543	41629	16055	1	0.049	0.071	0.100	0.161
50W	166067	84645	38516	16450	1	0.050	0.070	0.104	0.159
59NE	44085	19459	10987	4304	1	0.097	0.146	0.195	0.311
59NW	42730	20463	10360	4313	1	0.099	0.143	0.2	0.310
59SE	43723	19995	10032	4541	1	0.098	0.144	0.204	0.303
59SW	42051	20381	9571	4398	1	0.099	0.143	0.208	0.308
67N	15835	5845	3024.8	1299.3	1	0.162	0.267	0.371	0.566
67S	15772	5357	3125.2	1246.7	1	0.162	0.279	0.365	0.578
74N	3497	470.4	234.65	106.19	1	0.345	0.941	1.33	1.98
74S	3523	411.1	229.79	105.15	1	0.344	1.006	1.346	1.99
24NM64	1708.4 min^{-1}				8	0.022			

K is the conversion factor for the channels of the cosmic ray observation complex

Table 2

Averages of meteorological parameters and neutron monitor counting rate for each sample

Level, m.w.e.	Sample size *N*	Period	Atmospheric pressure, mb	Mass average temperature, °C	Surface temperature, °C	Monitor counting rate
0	956	01.05.16 12.12.18	1001.83	–29.86	–3.94	1708.40
7	1182	01.05.17 12.12.18	1001.20	–29.06	–2.69	1709.94
20	1077	01.01.16 12.12.18	1002.33	–30.86	–5.67	1701.97
40	1077	01.01.16 12.12.18	1002.33	–30.86	–5.67	1701.97

Table 3

Regression coefficients for channels of scintillation telescopes SMT00, SMT07, SMT20, and SMT40

Parameter	Depth, m.w.e.	Zenith angle, deg.				
		0	50	59	67	74
β, %/mb	00	–0.1470±0.0021	–0.1507±0.0023	–0.1817±0.0025	–0.2369±0.0031	–0.2730±0.0037
	07	–0.1430±0.0025	–0.1309±0.0028	–0.1306±0.003	–0.1175±0.0035	–0.1012±0.0041
	20	–0.0780±0.0019	–0.0785±0.002	–0.0741±0.0021	–0.0732±0.0024	–0.0684±0.0027
	40	–0.0766±0.0015	–0.0760±0.0012	–0.0592±0.0012	–0.0574±0.0013	–0.0535±0.0015
α_{ma}, %/°C	00	–0.3561±0.0053	–0.3276±0.0049	–0.3022±0.0045	–0.2387±0.0036	–0.2214±0.0032
	07	–0.1917±0.0034	–0.1778±0.0032	–0.1675±0.0030	–0.1572±0.0028	–0.1507±0.0027
	20	–0.1383±0.0025	–0.1245±0.0023	–0.1129±0.0021	–0.1087±0.0021	–0.0974±0.0019
	40	–0.1211±0.0024	–0.1018±0.0021	–0.0836±0.0017	–0.0539±0.0011	–0.0396±0.0008
γ	00	0.4634±0.007	0.3678±0.0083	0.3107±0.0089	0.2950±0.0091	0.2860±0.0095
	07	0.2548±0.0082	0.1692±0.0085	0.1544±0.009	0.1341±0.0098	0.1274±0.012
	20	0.2125±0.0084	0.1539±0.0088	0.1314±0.0095	0.1245±0.011	0.1226±0.014
	40	0.1887±0.0089	0.1203±0.0092	0.0966±0.011	0.0849±0.013	0.0592±0.016
$\alpha_{surf}\cdot 10^{-4}$, %/°C		–2.28±0.32	–2.51±0.41	–3.02±0.43	–2.6±0.68	–2.4±0.7

There are also regression coefficients in expression (1).: α_{surf} and α_{ma} are temperature coefficients for surface and mass average atmospheric temperatures respectively; β is the barometric coefficient; γ is the regression coefficient with neutron monitor data corrected for atmospheric pressure variations and reflecting primary CR variations. The coefficients α_{surf}, α_{ma}, β, γ in expression (1) were found as in [Yanchukovsky and Kuzmenko, 2018; Yanchukovsky, 2023], using the method of representing the regression equation on a standardized scale [Gorlach, 2006] and the least squares method [Korn, Korn, 1984]. The results are presented in Table 3.

In the period of interest (2016–2018), two Forbush decreases in cosmic rays were recorded (in July and September 2017), which were used to refine the regression coefficients γ. The temperature coefficient α_{surf} for a variable mass layer was verified using the method of paired correlation between $\Delta T_{\rm surf}(t)$ and the right-hand side of expression

$$\alpha_{\rm surf}\Delta T_{\rm surf}(t) = \frac{\delta J_{\rm surf}(t)}{h(t)-950} = \frac{\delta J_{\mu}(t) - \alpha_{\rm ma}\Delta T_{\rm ma}(t) - \beta\Delta h(t) - \lambda\delta J_{\rm n}(t)}{h(t)-950}. \quad (2)$$

From the solution of system of equations (1), all regression coefficients are found in the first approximation. Obtained α_{ma}, β, γ are substituted into (2), and the coefficients α_{surf} of the second approximation are derived, etc. This is dictated by the fact that the contribution of the variable mass layer to the total atmospheric temperature effect is very small (the regression coefficient for the mass average temperature α_{ma} is almost three orders of magnitude higher than α_{surf}). For a number of continuous data from 2016 to the end of 2018, α_{surf} was $-2.28\cdot 10^{-4}$ for the vertical with a correlation coefficient of –0.095, $\sigma_{\delta J_{\rm surf}(t)/(h(t)-950)} = 0.0482$, and $\sigma_{\Delta T_{\rm surf}(t)} = 20.052$.

The regression coefficients β, α_{surf}, α_{ma}, γ, listed in Table 3, allow us to identify the $\delta J_{\mu}(t)$ temperature component (integral temperature effect) in the observed muon intensity variations:

$$\delta I_{\mu T}(t) = \alpha_{\rm ma}\Delta T_{\rm ma}(t) = \delta J_{\mu}(t) - \beta\Delta h(t) - \alpha_{\rm surf}\Delta T_{\rm surf}(t) - \gamma\delta J_{\rm n}(t). \quad (3)$$

ANALYSIS METHODS IN USE

The Principal Component Analysis (PCA) (Aivazyan et al., 1989) is employed to extract relevant information from a large amount of multidimensional data [Jolliffe, 2002; Principal Manifolds..., 2007]. The raw data is represented as a rectangular matrix **X** with dimension of *I* rows and *J* columns. Rows of the matrix are called samples and are usually indicated by the index *i*, which varies from 1 to *I*. Variables are matrix columns that are usually designated by the index *j*=1, ..., *J*.

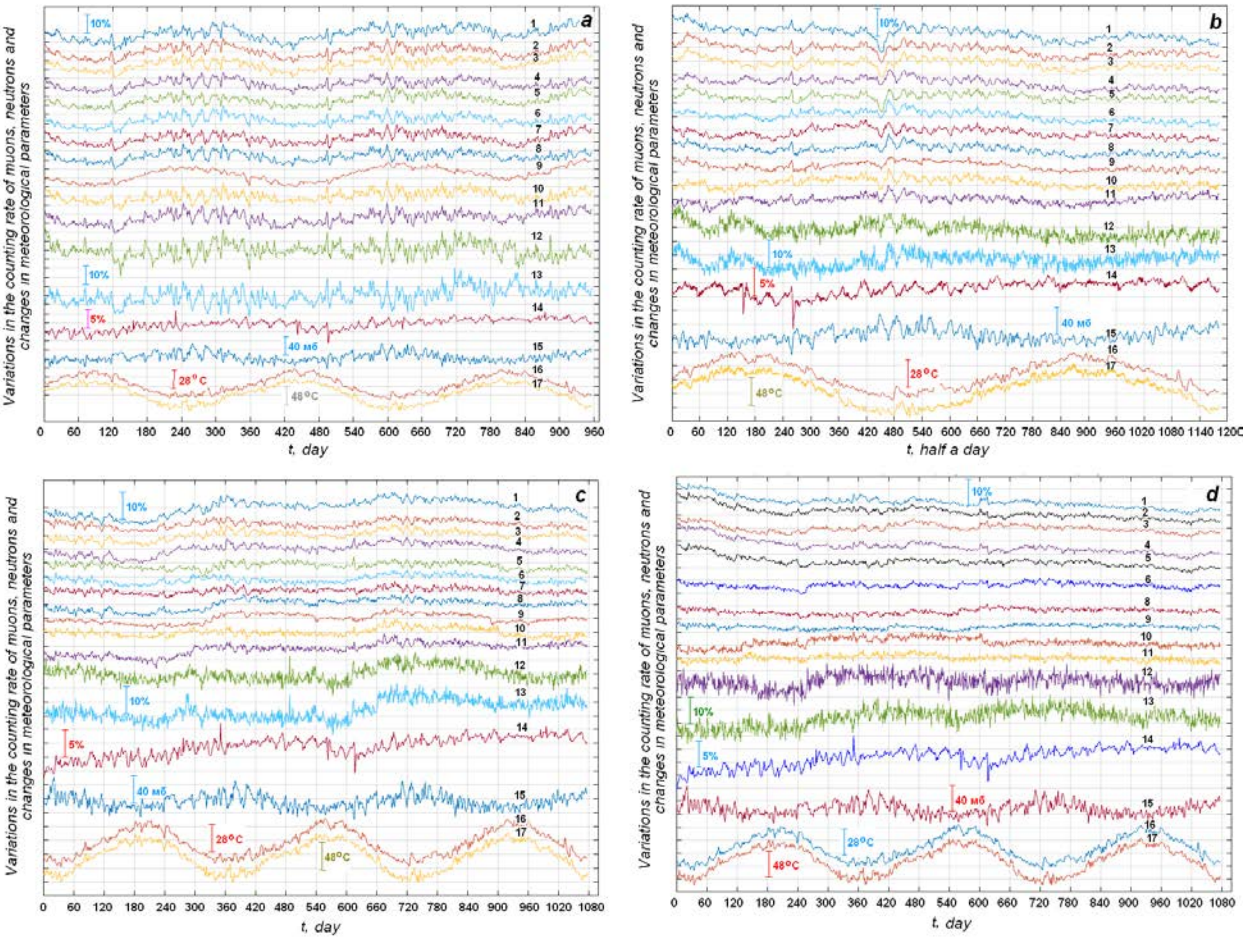

Figure 1. Muon counting rate variations, recorded by a scintillation telescope on the surface (*a*) and underground at depths of 7 (*b*), 20 (*c*), 40 m.w.e. (*d*) at zenith angles of 0° (curve 1), 50° from azimuthal directions N, S, E, W (curves 2–5 respectively), 59° from azimuthal directions NE, NW, SE, SW (curves 6–9 respectively), 67° from azimuthal directions N and S (curves 10 and 11), 74° from azimuthal directions N and S (curves 12 and 13), as well as neutron counting rate variations corrected for atmospheric pressure changes (curve 14), and atmospheric pressure changes (curve 15), mass average atmospheric temperature (curve 16), and variable mass layer temperature (curve 17)

Data dimension plays an important role in successful extraction of information. There is almost always noise in data. Its nature varies, and it is often a fraction of data that does not contain relevant information. Errors in raw data can lead to casual match between variables. In multidimensional data analysis using both methods of principal component regression and projections on latent structures, a space is constructed from a number of implicit parameters orthogonal to each other. Construction of such a space reduces to an orthogonal transformation into a new coordinate system as follows [Pomerantsev, 2014]:

- A new origin is defined as a data cloud center (performed by centering the raw data) and is taken as zero principal component;
- the sample variance of data along the first coordinate should be maximum (this coordinate is called the first principal component);
- the sample variance of data along the second coordinate is maximum under the condition of orthogonality to the first coordinate (the second principal component);
- The sample variance of data along the values of the *k*th coordinate is maximum provided it is orthogonal to the first $k-1$ coordinates.

The parent matrix of variables **X** has dimension ($I \times J$). Formally, new variables are introduced $\mathbf{t}_a = (a = 1, \ldots, A)$, which are a linear combination of original variables $\mathbf{x}_j = (j = 1, \ldots, J)$,

$$\mathbf{t}_a = \mathbf{p}_{a1}\mathbf{x}_1 + \ldots + \mathbf{p}_{aJ}\mathbf{x}_J. \quad (4)$$

As a result of the introduction of new variables, the parent matrix **X** is transformed into the product of matrices **T** and **P**:

$$\mathbf{X} = \mathbf{T}\mathbf{P}^{\mathbf{t}} + \mathbf{E} = \sum_{a=1}^{A} \mathbf{t}_a \mathbf{p}_a^t + \mathbf{E}. \quad (5)$$

The matrix **T** with dimension ($I \times A$) is called the counting matrix. The matrix **P** with dimension ($J \times A$) is said to be the load matrix. **E** is a matrix of residuals with dimension ($I \times J$). The score matrix **T** gives us the projections of the original samples (*j*-dimensional vectors **x**) onto the principal component subspace (*A*-dimensional). The rows of the matrix **T** are the coordinates of the samples in the new coordinate system. The columns of the matrix **T** are orthogonal and represent the projections of all samples onto one new coordinate axis. The loading matrix **P** is the transition matrix (transposition) from the original space of variables **x** (*j*-dimensional) to the principal component space (*A*-dimensional). Each row of the matrix **P** consists of coefficients linking the variables **t** and **x**. New variables $\mathbf{t}_a$ are referred to as principal components. The number of columns $\mathbf{t}_a$ in the **T** matrix and $\mathbf{p}_a$ in the **P** matrix is equal to the number of principal components *A*. The *A* value is significantly smaller than the number of variables *J* and the number of samples *I*. A distinctive feature of PCA should be considered the orthogonality of new variables (principal components). Consequently, as the number of matrix components increases, **T** and **P** are not rearranged, but a column corresponding to a new direction is added to each of them. To construct counts and loads, the recurrent algorithm NIPALS that finds one component at each step [Esbensen, 2005] is usually used. PCA is an iterative procedure in which components are added one after the other, sequentially. The question arises as to when to stop this process, i.e. how to find the optimal number of principal components *A*. If the *A* value is too small, the description of the data may be insufficient. An excessive *A* value leads to a situation where noise can be simulated. An important advantage of PCA is a significant reduction in data dimension. If the *A* dimension is chosen correctly, the **T** matrix contains as much information as it was in the original **X** matrix, which is much larger and more complex than the **T** matrix. When data *y* is involved in the decomposition of **X**, the PLS method allows us to obtain predicted results with a smaller number of PCs. The PLS method works like two PCAs performed for **X** and **Y**: $\mathbf{X} = \sum_A \mathbf{TP}^t + \mathbf{E}$ and $\mathbf{Y} = \sum_A \mathbf{UQ}^t + \mathbf{F}$ where **T**, **U** are counts, and **P**, **Q** are loads. PLS decomposition is carried out with regard to the close connection between the **X** and **Y** spaces. The projection is constructed consistently in order to maximize the correlation between the corresponding vectors of **X** counts $\mathbf{t}_a$ and **Y** counts $\mathbf{u}_a$. The raw data must first be centered and/or normalized before using PCA.

DATA ANALYSIS AND RESULTS

The temperature muon intensity variation, or the integral temperature effect of the atmosphere, occurs due to variation in the temperature of its different layers:

$$\delta J_{\mu T}(t_i) = \alpha_{\text{ma}} \Delta T_{\text{ma}}(t_i) = \sum_{j=1}^{16} \alpha_j \Delta T_j(t_i). \quad (6)$$

Here $\Delta T_j(t) = T_j(t) - \overline{T}_j$ are atmospheric temperature variations in the *j*th isobar, and α_j is the regression coefficient, or temperature coefficient, for the *j*th isobar.

In the analysis, as in [Yanchukovsky, 2023], we employed The Unscrambler X program [https://www.aspentech.com/en/products/apm/aspen-unscrambler], which can use PLS2 with four algorithms. The KERNEL PLS algorithm is optimum for such problems [Lindgren et al., 1993; De Jong, Ter Braak, 1994; Dayal, McGregor, 1997] since it is better suited than other algorithms for a large number of samples (thousands of samples with a large number of variables) [Yanchukovsky, Kuzmenko, 2018]. The raw data when prepared was centered and normalized. Centering involves searching for the data cloud center (zero principal component PC0). Centering is necessary because presented model (5) does not have a free term. The next step involves choosing the optimal number of principal components *A*. The choice of *A* corresponds to the boundary between the structural piece and noise of (5). Yanchukovsky [2023], when analyzing similar multidimensional data, has already used PCA, where the number of PCs was selected from the results obtained by calculating variances for selected PC vectors, eigenvalues of PC vectors, and the measure of informativeness of transformed data with increasing number of PCs. For clarity, when choosing the optimal number of principal components, it is recommended [Pomerantsev, 2014] to also leverage the residual plot. The PCA decomposition of the **X** matrix is an iterative process, and it can be interrupted at any step $a=A$. The resulting matrix $\hat{\mathbf{X}} = \mathbf{TP}^t$, generally differs from the **X** matrix. The difference between them $\mathbf{E} = \mathbf{X} - \hat{\mathbf{X}}$ is called the matrix of residuals. The *A* value can be verified [Yanchukovsky, 2023] when examining the variance of the residuals. As PCs are calculated and the resulting values are subtracted from the **X** matrix, the residuals change. These residuals are compared with $\mathbf{E}_0$ — the starting point in the equation $\mathbf{X}=\mathbf{TP}^{\mathbf{t}}+\mathbf{E}$, where $\mathbf{E}_0$ is **X**. It is convenient to express the residuals in relative units, using $\mathbf{E}_0$. For $A=0$, $\mathbf{E}=100$ % of $\mathbf{E}_0$. The residual plot thus obtained is exhibited in Figure 2, where a measure of informativeness of transformed data is presented for comparison.

The residual plot allows us to verify the optimal value of *A* in this problem. The slope (break) angle of curve describing the variance of residuals is virtually unchanged with the PC number $A \geq 2$, i.e. two PCs are sufficient to describe the structural piece of $\mathbf{TP}^{\mathbf{t}}$. This is the boundary between the structural piece, where the **T** matrix contains the basic information of the parent **X** matrix, and noise of the **E** matrix. In this case, the measure of informativeness is as great as 97.4 %. Thus, in this problem with two principal components, more than 95 % (97.4 %) of the initial variation is explained and the noise contribution is minimized.

The temperature coefficients α_j are related to the density of temperature coefficients by the ratio

$$w_j = \alpha_j \Delta h_i \Big/ \sum_{i=1}^{16} \Delta h_i. \quad (7)$$

The temperature coefficients α_j [%/°C] and densities of temperature coefficients w_j [%/°C·atm.] obtained by PLS2 for scintillation muon telescopes on the surface (SMT00) and underground at depths of 7 (SMT07), 20 (SMT20), and 40 m.w.e. (SMT40) at zenith angles of 0°, 50°, 59°, 67°, 74° are listed in Tables 4–8 respectively.

When switching from temperature coefficients to the density of temperature coefficients of muon intensity, a weight coefficient is taken into account which depends on the relative mass of each atmospheric layer $\Delta h_i \Big/ \sum_{i=1}^{16} \Delta h_i$.

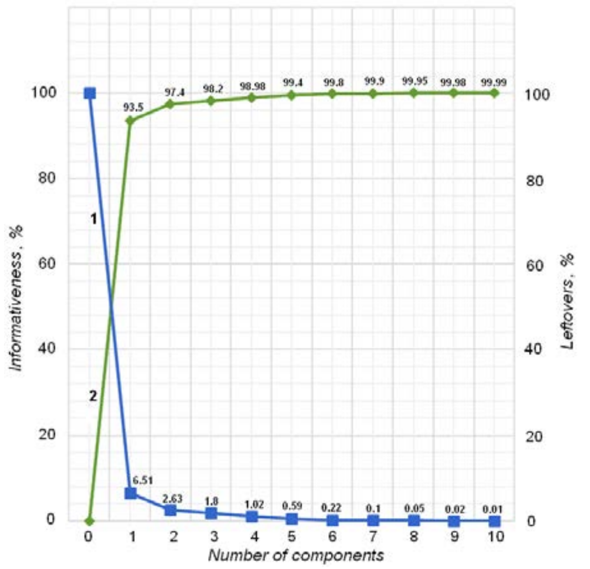

Figure 2. Variance of residuals (curve 1) and informativeness of transformed data (curve 2)

Density distributions of temperature coefficients w_j for muons in the atmosphere detected by scintillation telescopes at different zenith angles on the surface and underground are illustrated in Figure 3.

We believe that the observed distribution of the density of temperature coefficients for muons at atmospheric depths near 100 mb is caused by significant changes in the ratio between contributions of the negative temperature effect of muons and the positive temperature effect from the decay of pions at these atmospheric depths.

DISCUSSION

As in [Yanchukovsky, 2023], we assume that the integral temperature effect of muons in the atmosphere, found using the coefficient for the mass average atmospheric temperature and calculated taking into account the temperature coefficient density distribution from the data on the altitude temperature profile, will be the same within the limits of accuracy of estimated temperature coefficients. Accordingly, the average temperature coefficient density in the range from 0 to 950 mb should correspond to the coefficient for the mass average temperature. The results for comparison are presented in Table 8.

Within the given accuracy, all the results agree satisfactorily. The muon counting rate in the channels of scintillation telescopes is quite high (see Table 1), which ensures high statistical accuracy of muon detection (and reduces the noise level in raw data). This could have allowed us to choose a different boundary between

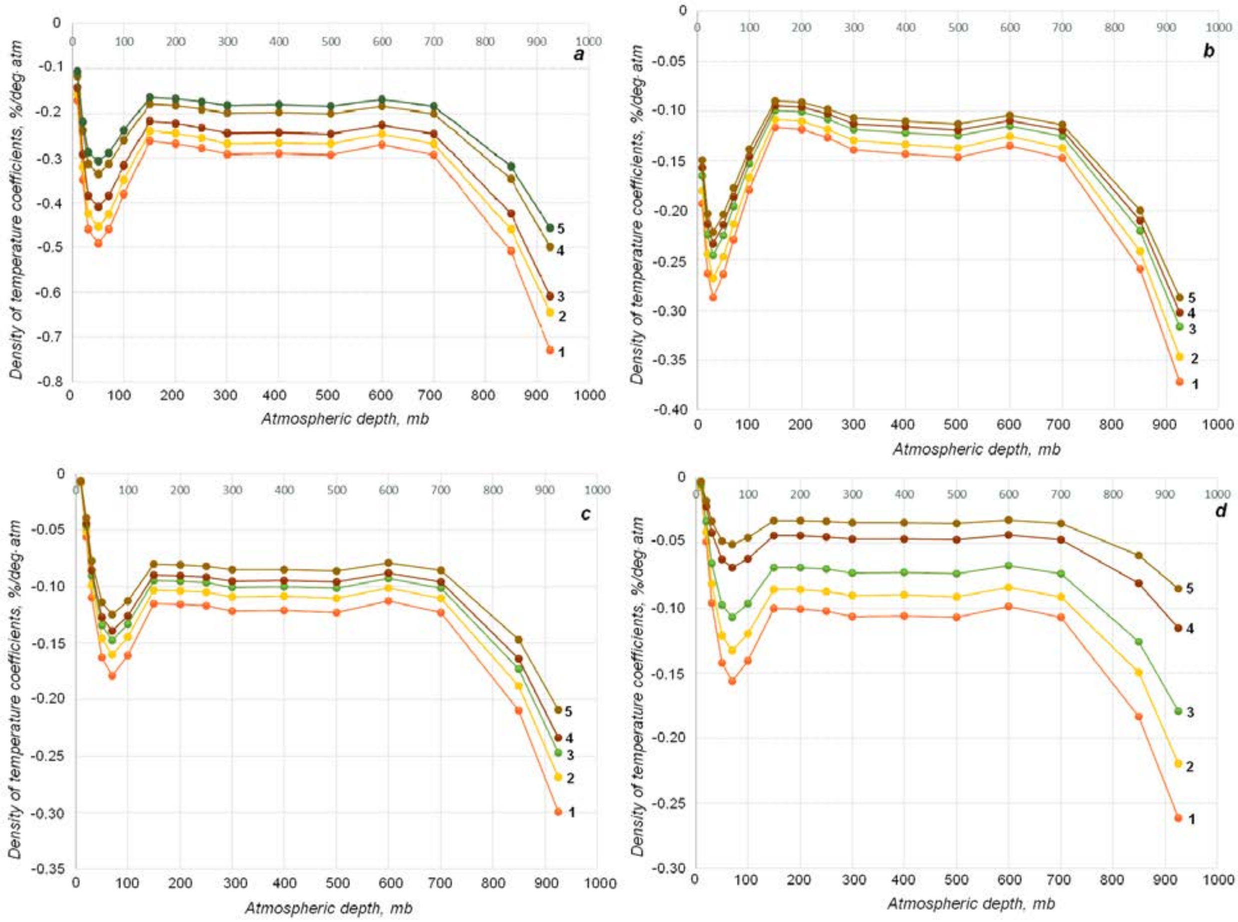

Figure 3. Density distributions of temperature coefficients for muons detected by scintillation telescopes on the surface (*a*) and underground at depths of 7 (*b*), 20 (*c*), and 40 m.w.e. (*d*) at zenith angles of 0° (curve 1), 50° (curve 2), 59° (curve 3), 67° (curve 4), and 74° (curve 5)

the structural piece of expression (5) and the matrix of residuals (noise) by increasing the number of principal components A to three, which would have further improved the accuracy of the final result.

However, noise in raw data is not only part of the data that does not contain the information you are looking for, not only random errors in the data, and casual match between variables, but also systematic errors caused by time variations in the efficiency of muon detection by scintillators. This necessitated correcting the raw data. That is why considering the real data (see Figure 2) led to the choice of no more than two principal components.

Table 4

Temperature coefficients and their densities
for the scintillation muon telescope SMT00 at different zenith angles

j	$h_{j,}$ mb	0° α_j $\times10^{-4}$	50° α_j $\times10^{-4}$	59° α_j $\times10^{-4}$	67° α_j $\times10^{-4}$	74° α_j $\times10^{-4}$	$\Delta h_{j,}$ mb	0° w_j $\times10^{-3}$	50° w_j $\times10^{-3}$	59° w_j $\times10^{-3}$	67° w_j $\times10^{-3}$	74° w_j $\times10^{-3}$
1	10	–27	–24	–24	–18	–17	15	–170	–155	–142	–116	–106
2	20	–37	–36	–31	–25	–23	10	–349	–319	–292	–238	–218
3	30	–72	–67	–61	–49	–45	15	–459	–424	–383	–313	–287
4	50	–103	–95	–86	–71	–65	20	–491	–453	–410	–335	–307
5	70	–97	–89	–81	–66	–61	20	–460	–425	–384	–314	–288
6	100	–180	–165	–150	–123	–113	45	–380	–349	–317	–260	–238
7	150	–137	–126	–115	–94	–86	50	–261	–239	–218	–178	–163
8	200	–141	–129	–117	–96	–88	50	–267	–245	–223	–182	–167
9	250	–146	–134	–122	–99	–92	50	–278	–255	–232	–190	–174
10	300	–230	–211	–192	–157	–144	75	–292	–267	–243	–199	–183
11	400	–305	–280	–255	–208	–191	100	–290	–266	–242	–198	–181
12	500	–309	–283	–259	–211	–193	100	–293	–268	–246	–200	–183
13	600	–283	–259	–238	–193	–177	100	–269	–246	–226	–184	–168
14	700	–463	–424	–389	–316	–293	150	–293	–269	–247	–200	–183
15	850	–535	–483	–447	–365	–335	100	–509	–459	–424	–347	–318
16	925	–383	–339	–320	–262	–240	50	–729	–644	–608	–498	–456

Table 5

Temperature coefficients and their densities
for the scintillation muon telescope SMT07 at different zenith angles

j	$h_{j,}$ mb	0° α_j $\times10^{-4}$	50° α_j $\times10^{-4}$	59° α_j $\times10^{-4}$	67° α_j $\times10^{-4}$	74° α_j $\times10^{-4}$	$\Delta h_{j,}$ mb	0° w_j $\times10^{-3}$	50° w_j $\times10^{-3}$	59° w_j $\times10^{-3}$	67° w_j $\times10^{-3}$	74° w_j $\times10^{-3}$
1	10	–30	–28	–26	–25	–24	15	–193	–180	–165	–157	–149
2	20	–28	–26	–24	–22	–21	10	–263	–243	–224	–214	–203
3	30	–45	–42	–39	–37	–35	15	–287	–268	–245	–233	–222
4	50	–56	–52	–47	–45	–43	20	–264	–246	–225	–214	–204
5	70	–48	–45	–41	–39	–37	20	–229	–214	–195	–186	–177
6	100	–85	–79	–72	–69	–66	45	–179	–167	–153	–146	–139
7	150	–61	–57	–52	–50	–47	50	–117	–109	–99	–95	–90
8	200	–62	–58	–53	–51	–48	50	–119	–111	–101	–96	–92
9	250	–67	–62	–57	–54	–52	50	–127	–118	–108	–103	–98
10	300	–110	–102	–93	–89	–85	75	–139	–130	–118	–113	–107
11	400	–151	–140	–128	–122	–116	100	–143	–133	–122	–116	–110
12	500	–154	–144	–132	–125	–119	100	–147	–137	–125	–119	–113
13	600	–142	–132	–121	–115	–110	100	–135	–126	–115	–109	–104
14	700	–233	–217	–198	–188	–179	150	–147	–137	–126	–120	–114
15	850	–272	–254	–232	–221	–210	100	–258	–241	–220	–210	–200
16	925	–196	–182	–167	–159	–151	50	–372	–347	–317	–302	–287

Table 6

Temperature coefficients and their densities
for the scintillation muon telescope SMT20 at different zenith angles

j	h_j, mb	0° α_j $\times10^{-4}$	50° α_j $\times10^{-4}$	59° α_j $\times10^{-4}$	67° α_j $\times10^{-4}$	74° α_j $\times10^{-4}$	Δh_j, mb	0° w_j $\times10^{-3}$	50° w_j $\times10^{-3}$	59° w_j $\times10^{-3}$	67° w_j $\times10^{-3}$	74° w_j $\times10^{-3}$
1	10	–1.3	–1.2	–1.1	–1	–0.9	15	–8	–7.5	–6.8	–6.5	–5.8
2	20	–5.9	–5.3	–4.8	–4.6	–4.1	10	–56	–50	–46	–44	–39
3	30	–17	–15	–14	–13	–12	15	–110	–98	–90	–86	–77
4	50	–34	–31	–28	–27	–24	20	–162	–146	–134	–127	–113
5	70	–38	–34	–31	–29	–26	20	–178	–160	–147	–139	–125
6	100	–76	–68	–63	–59	–53	45	–161	–144	–133	–125	–112
7	150	–60	–54	–50	–47	–42	50	–115	–103	–95	–89	–80
8	200	–61	–54	–50	–47	–42	50	–115	–103	–95	–90	–81
9	250	–62	–55	–51	–48	–43	50	–117	–105	–96	–91	–82
10	300	–96	–86	–79	–75	–67	75	–121	–109	–100	–95	–85
11	400	–127	–114	–105	–99	–89	100	–121	–109	–100	–94	–85
12	500	–129	–116	–106	–101	–90	100	–123	–110	–101	–96	–86
13	600	–118	–106	–98	–92	–83	100	–113	–101	–93	–88	–79
14	700	–193	–173	–158	–151	–135	150	–122	–110	–101	–96	–86
15	850	–221	–198	–182	–172	–154	100	–209	–188	–173	–163	–146
16	925	–157	–141	–130	–123	–110	50	–299	–268	–246	–233	–209

Table 7

Temperature coefficients and their densities
for the scintillation muon telescope SMT40 at different zenith angles

j	h_j, mb	0° α_j $\times10^{-4}$	50° α_j $\times10^{-4}$	59° α_j $\times10^{-4}$	67° α_j $\times10^{-4}$	74° α_j $\times10^{-4}$	Δh_j, mb	0° w_j $\times10^{-3}$	50° w_j $\times10^{-3}$	59° w_j $\times10^{-3}$	67° w_j $\times10^{-3}$	74° w_j $\times10^{-3}$
1	10	–1.1	–1	–0.8	–0.5	–0.4	15	–7.2	–6.1	–5	–3.2	–2.3
2	20	–5.1	–4.4	–3.5	–2.3	–1.9	10	–49	–42	–33	–22	–18
3	30	–15	–13	–10	–6.7	–5.3	15	–96	–82	–66	–42	–34
4	50	–30	–25	–21	–13	–10	20	–142	–121	–97	–63	–49
5	70	–33	–28	–23	–15	–11	20	–156	–133	–107	–69	–51
6	100	–67	–57	–46	–29	–22	45	–141	–120	–96	–62	–46
7	150	–53	–45	–36	–23	–17	50	–100	–85	–69	–44	–33
8	200	–53	–45	–36	–23	–17	50	–101	–86	–69	–44	–33
9	250	–54	–46	–37	–24	–17	50	–102	–87	–70	–45	–33
10	300	–84	–71	–57	–37	–27	75	–106	–90	–73	–47	–34
11	400	–111	–95	–76	–49	–36	100	–106	–90	–73	–47	–34
12	500	–113	–96	–77	–50	–37	100	–107	–91	–74	–47	–35
13	600	–104	–88	–71	–46	–34	100	–99	–84	–68	–44	–32
14	700	–169	–144	–116	–75	–55	150	–107	–91	–73	–47	–35
15	850	–193	–157	–132	–85	–63	100	–183	–150	–126	–81	–59
16	925	–138	–115	–94	–61	–45	50	–261	–219	–179	–116	–85

Table 8

Comparison between temperature coefficients

Zenith angle		0°	50°	59°	67°	74°
SMT00	$\overline{w_i}$	–0.3619 ± 0.0094	–0.3302 ± 0.0085	–0.3024 ± 0.0078	–0.247 ± 0.0064	–0.2264 ± 0.0059
	α_{ma}	–0.3561 ± 0.0053	–0.3276 ± 0.0049	–0.3022 ± 0.0045	–0.2387 ± 0.0036	–0.2214 ± 0.0032
SMT07	$\overline{w_i}$	–0.1950 ± 0.005	–0.1711 ± 0.0044	–0.1661 ± 0.0043	–0.1583 ± 0.0041	–0.1505 ± 0.0039
	α_{ma}	–0.1917 ± 0.0034	–0.1778 ± 0.0032	–0.1675 ± 0.0030	–0.1572 ± 0.0028	–0.1507 ± 0.0027
SMT20	$\overline{w_i}$	–0.1331 ± 0.0034	–0.1195 ± 0.003	–0.1097 ± 0.0028	–0.1038 ± 0.0027	–0.0931 ± 0.0024
	α_{ma}	–0.1383 ± 0.0025	–0.1245 ± 0.0023	–0.1129 ± 0.0021	–0.1087 ± 0.0021	–0.0974 ± 0.0019
SMT40	$\overline{w_i}$	–0.1165 ± 0.003	–0.0986 ± 0.0025	–0.0799 ± 0.002	–0.0515 ± 0.0013	–0.0383 ± 0.0010
	α_{ma}	–0.1211 ± 0.0024	–0.1018 ± 0.0021	–0.0836 ± 0.0017	–0.0539 ± 0.0011	–0.0396 ± 0.0008

The results obtained by analyzing the observational data were compared with the results of calculation of expected temperature coefficient densities for the complex of underground muon telescopes in Yakutsk, we have carried out in [Kuzmenko, Yanchukovsky, 2017] for zenith angles of 0°, 30°, and 60°. Figure 4 shows the results obtained for zenith angles of 0° and 60° (59°) at four observation levels of 0, 7, 20, and 40 m.w.e. for comparison.

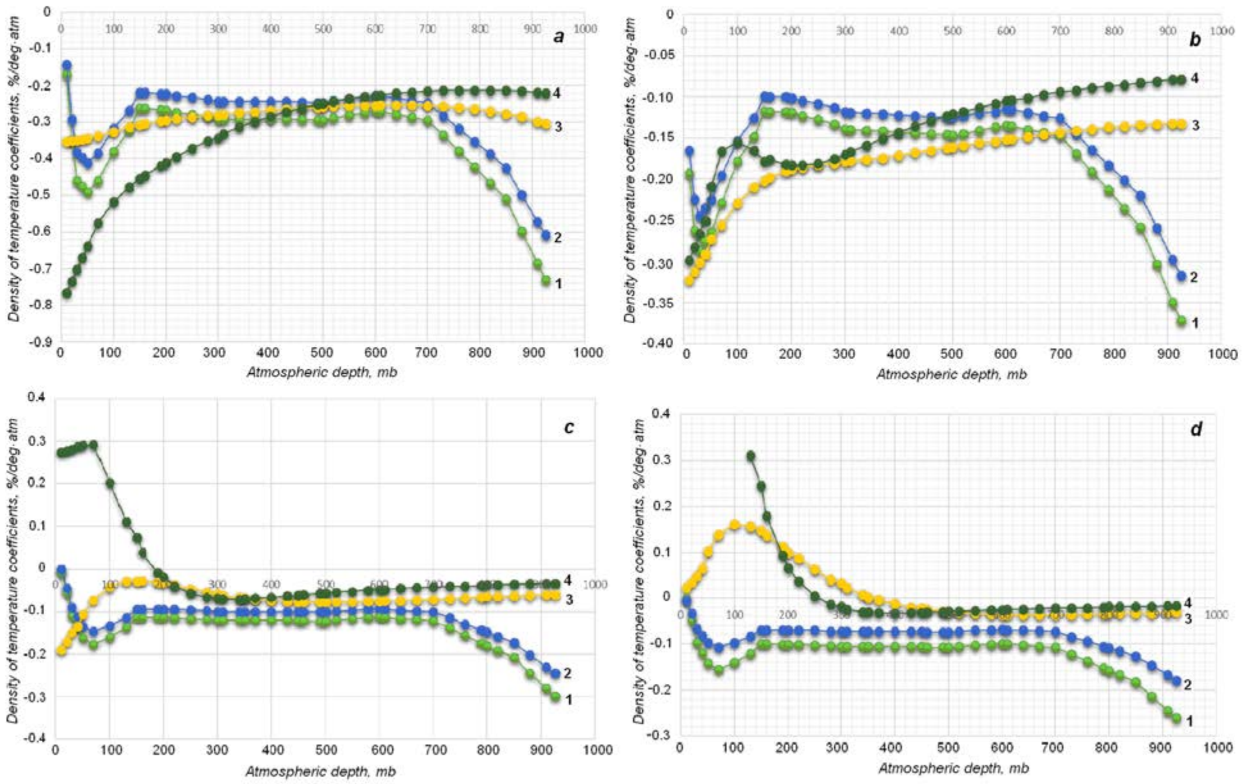

Figure 4. Density distributions of temperature coefficients in the atmosphere for muons recorded at the levels of 0 (*a*), 7 (*b*), 20 (*c*), and 40 m.w.e. (*d*) at zenith angles of 0° (curve 1) and 59° (curve 2), found by analyzing observational data, as well as density distributions of temperature coefficients obtained by calculating expected values for zenith angles of 0° (curve 3) and 60° (curve 4)

The expected values have been calculated in [Kuzmenko et al., 2017] when scintillation telescopes had not yet been put into operation. That is why the 0° and 60° angles were included in the calculations. There is a qualitative agreement between the results of the analysis of observational data and theoretical calculations. The reliability of experimental results depends on the quality and amount of initial experimental data (and it is assessed). The results obtained by calculation should be treated more carefully since the calculation has to be made with a large variety of assumptions.

It is interesting to compare the results obtained by similar analysis methods for two underground complexes of muon telescopes — with scintillation and gas-discharge counters [Yanchukovsky, 2023]. Figure 5 illustrates density distributions of temperature coefficients in the atmosphere for muons detected from the vertical direction underground by telescopes of these types.

The results presented in Figure 5 indicate that the temperature effect of muons in the atmosphere decreases as their energy increases. Accordingly, data from only one, vertical, direction of muon detection by tele scopes of both types is quite sufficient to diagnose the thermobaric regime of the atmosphere by cosmic rays [Yanchukovsky, 2020]. SMTs provide high statistical

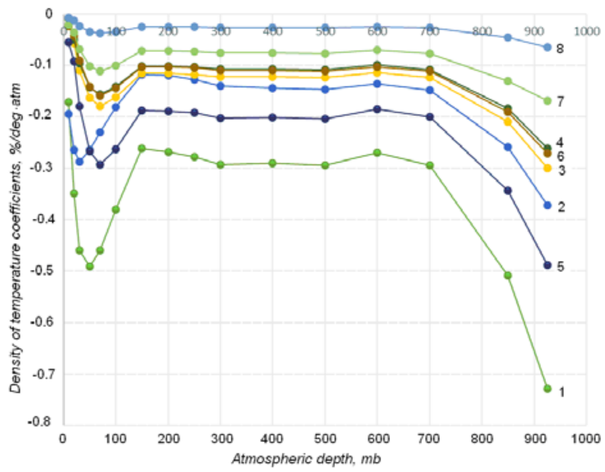

Figure 5. Density distribution of temperature coefficients in the atmosphere for muons detected from the vertical direction at the levels of 0, 7, 20, and 40 m.w.e. by scintillation telescopes (curves 1–4 respectively) and telescopes with gas-discharge counters (curves 5–8 respectively)

accuracy of muon intensity detection as compared to MT, but are significantly inferior to them in stability of detection efficiency.

Thus, SMT and MT do not duplicate, but complement each other, expanding the capabilities of the A.I. Kuzmin Cosmic Ray Spectrograph in Yakutsk.

CONCLUSION

We have found density distributions of temperature coefficients for muons detected with scintillation telescopes on the surface and underground, using PCA of continuous observations.

The experimental estimation of the density distribution of temperature coefficients makes it possible to effectively take into account the temperature effect in observational data from scintillation telescopes.

Comparison of the results obtained by analyzing experimental data with the results of calculation of expected temperature coefficient densities suggests that they agree satisfactorily.

By comparing the results received by similar analysis methods for muon telescopes with gas-discharge and scintillation counters, we have concluded that the simultaneous use of muon telescopes of these types in the Yakutsk complex expands the energy range of detected cosmic rays. Scintillation telescopes provide high statistical accuracy in recording the muon intensity compared to telescopes with gas-discharge counters, but they are significantly inferior to them in the stability of detection efficiency. They complement each other, expanding the capabilities of the A.I. Kuzmin Cosmic Ray Spectrograph in Yakutsk.

The work was financially supported by the Ministry of Science and Higher Education of the Russian Federation (Project FWZZ-2022-0019). The results were obtained using the equipment of the Unique Research Facility "Russian National Network of Cosmic Ray Stations" [http://www.ckp-rf.ru/usu/433536].

REFERENCES

Aivazyan S.A., Buhshtaber V.M., Enyukov I.S., Meshalkin L.D. *Prikladnaya Statistika. Klassifikatsiya i snizhenie razmernosti* [Applied statistics. Classification and dimension lowering]. Moscow, Finansy i statistika Publ., 1989, p. 607. (In Russian).

Dayal B.S., McGregor J.F. Improved PLS algorithms. *J. Chemometrics*. 1997, vol. 11, pp. 73–65.

De Jong S., Ter Braak C. Comments on the PLS kernel algorithm. J. *Chemometrics*. 1994, vol. 8, pp. 169–174.

Esbensen K. *Analysis of Multidimensional Data. Selected Chapters*. Chernogolovka, IPHF RAN Publ., 2005, 160 p. (In Russian).

Gerasimova S.K., Gololobov P.Yu., Grigor'ev V.G., Zverev A.S., Starodubtsev S.A., Egorov A.G., Neustroev N.I., Mikheev A.A., Sorokin E.E., Karmadonov A.Ya., Pakhmulov A.V. Muon telescope on scintillation counters.*Pribory i tekhnika etksperimenta* [Instruments and experimental technique]. 2021, no. 4, pp. 65–73. (In Russian).

Gorlach B.A. *Matematika* [Mathematics]. Moscow, Nauka Publ., 2006, 911 p. (In Russian).

Grigoryev V.G., Starodubtsev S.A., Krymsky G.F., Krivoshapkin P.A., Timofeev V.E., Prikhodko A.N., Karmadonov A.Ya. Modern Yakutsk Cosmic Ray Spectrograph after A.I. Kuzmin. *Proc. 32nd International Cosmic Ray Conference, Beijing, 2011*, vol. 11, pp. 252–255, id0360. DOI: 10.7529/ICRC2011/V11/0360.

Jolliffe I.T. *Principal Component Analysis*. New York, Springer, 2002, 516 p. (Springer Series in Statistics).

Korn G., Korn T. *Spravochnik po matematike dlya nauchnykh rabotnikov i inzhenerov* [A Handbook of Mathematics for Scientists and Engineers]. Moscow, Nauka Publ., 1984, 831 p. (In Russian). (English edition: Korn G., Korn T. Mathematical Handbook for Scientists and Engineers. New York, McGraw-Hill Inc., 1968, 1130 p.)

Kuzmenko V.S., Yanchukovsky V.L. Determination of the density of temperature coefficients for muons in the atmosphere. *Solnechno-zemnaya fizika* [Solar-Terrestrial Physics]. 2015, vol. 1, no. 2, pp. 91–96. (In Russian). DOI: 10.12737/10403.

Kuzmenko V.S., Yanchukovsky V.L. Distribution of temperature coefficient density for muons in the atmosphere. *Solar-Terrestrial Physics*. 2017, vol. 3, iss. 4, pp. 104–116. DOI: 10.12737/stp-34201710.

Lindgren F., Geladi P., Wold S. The kernel algorithm for PLS. *J. Chemometrics*. 1993, vol. 7, pp. 45–59. DOI: 10.1002/cem.1180070104.

Pomerantsev A.L. *Khemometrika v Excel: uchebnoe posobie.* [Chemometrics in Excel: Tutorial]. Tomsk, TPU Publ., 2014, 435 p. (In Russian).

Principal Manifolds for Data Visualization and Dimension Reduction / Gorban A.N., Kegl B., Wunsch D., Zinovyev A.Y. (Eds). Berlin; Heidelberg; New York, Springer, 2007, 364 p. (Lecture Notes in Computational Science and Engineering, vol. 58).

Shapley A.H. *Guide to International Data Exchange in Solar-Terrestrial Physics* / IUCSTP Working Group 1. Budapest, 1969, p. 5.

Starodubtsev S.A., Grigor'ev V.G., Isakov D.D., Karmadonov A.Ya., Pakhmulov A.V., Egorov A.G., Ksenofontov I.V. Modernization of the Yakutsk Cosmic Ray Spectrograph named after A.I. Kuzmin. *Proc. All-Russian Conference on Solar-Terrestrial Physics, dedicated to the 100th anniversary of the birth of Corresponding Member of the Russian Academy of Sciences V.E. Stepanov*, Irkutsk, ISZF SO RAN Publ., 2013, pp. 289–293. (In Russian).

Starodubtsev S.A., Grigor'ev V.G., Gololobov P.Yu. Yakutsk Cosmic Ray Spectrograph named after A.I. Kuzmin: Current state. *Proc. All-Russian Conference "Heliogeophysical Research in the Arctic"*] Murmansk, Polar Geophysical Institute Publ., 2016, pp. 125–129. (In Russian).

Yanchukovsky V.L. Muon intensity variations and atmospheric temperature. *Solar-Terrestrial Physics*. 2020, vol. 6, iss. 1, pp. 108–115. DOI: 10.12737/stp-61202013.

Yanchukovsky V. Temperature effect of muons registered under the ground in Yakutsk by telescopes on gas-discharge counters. *Solar-Terrestrial Physics*. 2023, vol. 9, no. 2, pp. 55–65. DOI: 10.12737/stp-92202307.

Yanchukovsky V.L., Filimonov G.Ya. *Variatsii neitronnoi komponenty kosmicheskikh luchei* [Variations in the neutron component of cosmic rays]. Preprint no. 1. Novosibirsk, OIGGiM SO AN SSSR Publ., 1994, 11 p. (In Russian).

Yanchukovsky V.L., Kuzmenko V. Atmospheric effects of the cosmic-ray mu-meson component. *Solar-Terrestrial Physics*. 2018, vol. 4, iss. 3, pp. 76–82. DOI: 10.12737/stp-43201810.

URL: https://ikfia.ysn.ru/dannye-lklve (accessed November 15, 2024).

URL: https://ikfia.ysn.ru/data/hecrlab/mt (accessed November 15, 2024).

URL: https://ikfia.ysn.ru/data/hecrlab/ipm (accessed November 15, 2024).

URL: https://www.nco.ncep.noaa.gov/pmb/products/gfs (accessed November 15, 2024).

URL: https://www.aspentech.com/en/products/apm/aspen-unscrambler (accessed November 15, 2024).

URL: http://www.ckp-rf.ru/usu/433536 (accessed November 15, 2024).

Original Russian version: Yanchukovsky V.L., Khisamov R.Z., published in Solnechno-zemnaya fizika. 2025, vol. 11, no. 1, pp. 98–108. DOI: 10.12737/szf-111202511. © 2025 INFRA-M Academic Publishing House (Nauchno-Izdatelskii Tsentr INFRA-M)

How to cite this article

Yanchukovsky V.L., Khisamov R.Z. Temperature effect of muons detected underground by scintillation detectors. *Solar-Terrestrial Physics*. 2025, vol. 11, iss. 1, pp. 90–100. DOI: 10.12737/stp-111202511.